*Journal of Nepal Geological Society, 2002, Vol. 26, pp. 17–27*

# Estimating streaming potentials associated with geothermal circulation at the Main Central Thrust: an example from Tatopani-Kodari hot spring in central Nepal

***Frédéric Perrier[1], Gyani Raja Chitrakar[2], Thierry Froidefond[1], Dilliram Tiwari[2], Umesh Gautam[1], Basanta Kafle[2] and Michael Trique[1]**

[1]*Département Analyse, Surveillance, Environnement, Commissariat à l'Energie Atomique, BP12, F-91680 Bruyères-Le-Châtel, France*

*(*Corresponding author, e-mail: perrier@dase.bruyeres.cea.fr)*

[2]*National Seismological Centre, Department of Mines and Geology, Lainchaur, Kathmandu, Nepal*

## ABSTRACT

Streaming potential coefficient and electrical conductivity have been measured in the laboratory as a function of KCl electrolyte conductivity for six crushed rock samples collected at the Main Central Thrust (MCT) zone, near the Tatopani-Kodari hot spring in Central Nepal. Surface conductivity values range from 0.11±0.07 to 1.19±0.13 mS/m and values of the inferred ζ potential vary from -16.3±0.2 mV to -41.2±1.0 mV. These experimental values are used to model the streaming potential coefficient and the rock resistivity as a function of permeability. The electric potential generated on surface by the geothermal circulation at the MCT zone is then derived using a simple two-dimensional analytical calculation. The maximum expected anomaly depends on the values of poorly known parameters such as the permeability of the MCT but is estimated to be of the order of 20 mV, and in general tends to remain below 100 mV. Such anomalies, although they could reflect variations of crustal parameters associated with stress accumulation, are difficult to detect and do not appear as a promising possibility in the search for earthquake precursors.

## INTRODUCTION

Streaming potentials are electrical potential differences produced when an electrolyte is flowing in a porous medium (e.g. Ishido and Mizutani 1981; Revil et al. 1999a; Marino et al. 2000). The application of streaming potentials for the detection of groundwater circulation in geophysical systems was demonstrated many decades ago, for example to study the leakage of earth dams (Ogilvy et al. 1969; Bogoslovsky and Ogilvy 1970). Streaming potentials were therefore proposed as a possible method to detect groundwater flow associated with the precursory phase of an earthquake (Mizutani et al. 1976). Though examples of time variations of the electric potential occurring before large earthquakes have been reported (e.g. Raleigh et al. 1977; Corwin and Morrison 1977), and streaming potentials suggested as an explanation, the relationship to the earthquakes has not been demonstrated. The enthusiasm of the late seventies was actually followed by growing scepticism, mostly because of the hot debate around the controversial prediction method (see for example the special issue of Geophys. Res. Lett. edited by Geller in 1996) advertised in Greece by Varotsos and coworkers (Varotsos et al. 1993). In general, indeed, electrical signals are difficult to interpret because of many artefacts of meteorological (Corwin and Hoover 1979) or industrial origin (Pham et al. 1998; Pham et al. 2001).

Studies on the structure of the Spontaneous Potential (SP) in geothermal areas (e.g. Zohdy et al. 1973; Massenet and Pham 1985) and the observation of electric or magnetic signals in association with volcanic eruptions (e.g. Zlotnicki and Le Mouël 1990; Michel and Zlotnicki 1998) however, indicate that streaming potentials are relevant and practical. Recently, streaming potentials have therefore been the subject of a renewed interest. In the laboratory, the streaming potential coefficient (SPC) of various rocks has been measured for crushed samples (Lorne et al. 1999a) and intact samples (e.g. Yoshida 2001; Jouniaux et al. 2000; Pengra et al. 1999; Lorne et al. 1999b; Jouniaux and Pozzi 1995). In the field, streaming potentials have been studied in the vicinity of artificial lakes (Perrier et al. 1998; Trique et al. 1999), an intermittent spring (Perrier et al. 1999), in underground quarries (Morat et al. 1989; Morat and Le Mouël 1992), in walls of historical monuments (Pisarenko et al. 1996) or in the soil (Thony et al. 1997; Perrier and Morat 2000). Detailed theoretical estimates of streaming potentials were also undertaken for geothermal systems (Revil and Pezard 1998; Revil et al. 1999b; Ishido and Pritchett 1999; Adler et al. 1999) or accretionary prisms (Jouniaux et al. 1999).

No estimates of streaming potentials have been attempted so far in the context of a continental collision zone, such as the Himalayas of Nepal. Also, not much is known about the electrical parameters of the Himalayan rocks. This region is

important to study because it is seismically active (Pandey et al. 1999) and exhibits a deficit of large magnitude earthquakes (Bilham et al. 1998). Furthermore, a magneto-telluric survey (Lemonnier et al. 1999) evidenced a conductor associated with a stress accumulation zone located south of the MCT (Pandey et al. 1995). If water is present at the epicentral zone, then streaming potentials may be generated during the preparation phase of the large Himalayan earthquakes. Groundwater circulation is also present at the MCT, as illustrated by the numerous hot springs observed along the Himalayan arc (Bhattarai 1980). Stress variations during the seismic cycles may lead to changes in the crustal properties, leading tochanges in the geothermal circulation at the MCT.

In this paper, a first estimate of streaming potentials associated with geothermal circulation at the MCT is presented. The electrical parameters of six rock samples typical of the MCT zone have been measured in the laboratory. These results are used to model the expected rock resistivity and SPC as a function of permeability. The structure of SP resulting from the geothermal circulation is then obtained from a simple two-dimensional analytical calculation.

## CONTEXT OF THE STUDY

Geothermal circulation in the Himalayan belt is still poorly constrained. For the purpose of this paper, we shall assume that the hot springs correspond to the exit points of meteoric water recharged on the High Himalaya and the Tibetan plateau (Fig. 1). Geothermal circulation meets high temperatures at depth (Cattin et al. 2001) and is then drained by the MCT to the surface. Although the MCT is not currently active (Upreti 1999; Pandey et al. 1999), it still corresponds to a major zone of increased permeability in the brittle crust. In the simple model depicted in Fig. 1, water circulation results from both thermal buoyancy forces and topographic gradient.

Rock samples were collected at the MCT zone near the hot spring of Tatopani-Kodari (Fig. 2). This hot spring has a temperature of about 40°C and a flow rate measured to be 3±0.2 liter/s in February 2000. A larger value (5 liter/s) was reported earlier (Bhattarai 1980) but it is hard to estimate at this time if this difference is significant, and whether it provides an indication for significant time dependence of the flow rate. Electrical conductivity of the water is high (847 µS/cm), corresponding to a low resistivity of 12 Ωm. Compared with geothermal circulation in volcanic areas (Revil and Pezard 1998), the pH of the water is close to neutrality (Table 1). Other hot springs located at the MCT zone in central Nepal, such as the springs in Syabru Bensi or Chilime, have similar characteristics (see Table 1), and the Tatopani-Kodari spring can be considered as a representative average. The dispersion of the values of the temperature or electrical conductivity, for the various springs, or for the various exhausts of the same spring in Syabru-Bensi, suggests that the deep geothermal waters are mixed with cold subsurface meteoric aquifers, as is observed for other geothermal systems (Vasseur et al. 1997).

Representative fresh rock samples were taken from outcrops. Five samples were collected north of the MCT in the Himalayan gneiss, and one was taken in a phyllite bed in the Deurali Limestone unit (Fig. 2). The mineralogy of the samples was studied by X-ray diffraction and is reported in Table 2. All samples are quartz-muscovite gneiss with varying grades and varying amounts of feldspar and amphibole, typical of the Higher Himalayan Crystallines and Lesser Himalayan Gneiss (Upreti 1999; Guillot 1999).

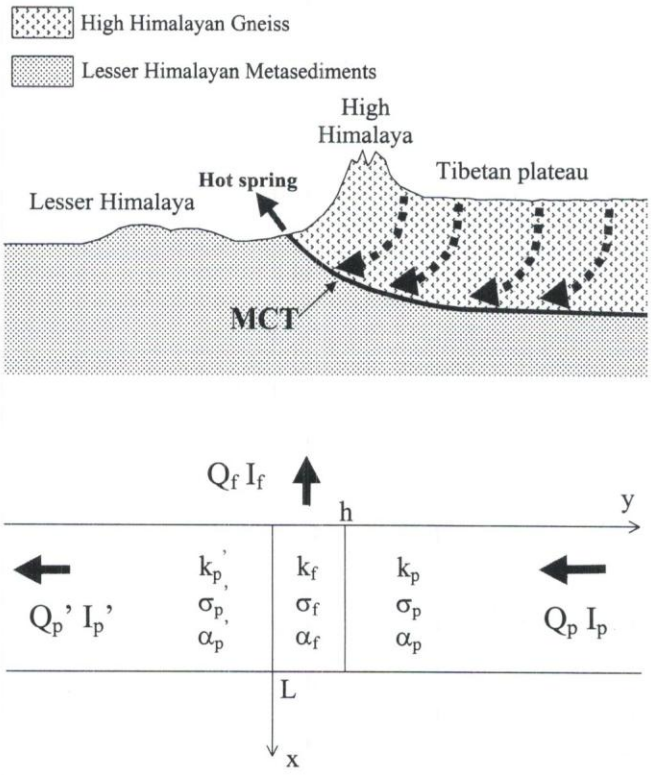


**Fig. 1: Sketch of the simple model of geothermal circulation considered in this paper. Hot springs are produced by meteoric water recharged in the High Himalayas and the Tibetan plateau, and drained by the MCT to the surface. The bottom sketch shows the simple 2-D model of the MCT zone used for the analytical calculation of the combined water flow and electrical current. The MCT is represented by a fractured slab of height $L$ and width $h$ with permeability $k_f$, electrical conductivity $\sigma_f$ and electroosmotic coupling $\alpha_f$. This slab is inserted between two porous media p and p' of permeability $k_p$ and $k_p$', electrical conductivity $\sigma_p$ and $\sigma_p$' and electroosmotic couplings $\alpha_p$ and $\alpha_p$'. Boundary conditions are given by flow rates $Q_f$, $Q_p$ and $Q_p$', and total electric currents $I_f$, $I_p$ and $I_p$'. No water flow or electric current is assumed to cross the boundary $x=L$ and across $x=0$ for $y<0$ and $y>h$.**

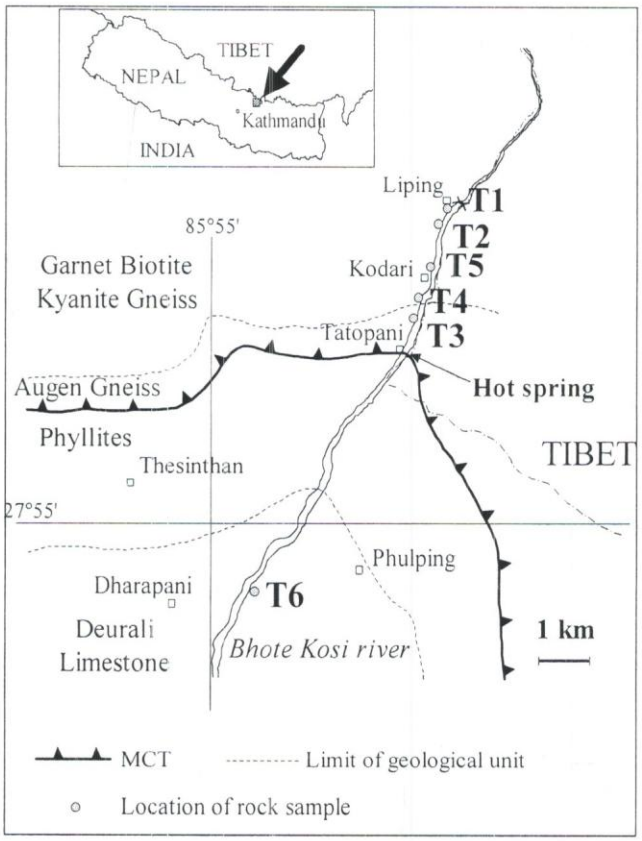


**Fig. 2: Geological map of the Tatopani-Kodari area showing the location of the rock samples used in the present study (after Madhikarmi 1980).**

## LABORATORY MEASUREMENTS

Samples were crushed and saturated with KCl solutions of varying concentration. The electrical conductivity was measured as a function of the conductivity of the KCl solution with an experimental set-up described in detail in Lorne et al. (1999a). Typical results are shown in Fig. 3 for samples T3 and T6. The sample electrical conductivity $\sigma_r$ as a function of electrolyte conductivity $\sigma_f$ is described by the RG equation (Revil and Glover 1998; Revil et al. 1999b) :

$$\sigma_r = \frac{\sigma_f}{F_0} H\left(\frac{\sigma_s}{\sigma_f}\right) \quad (1)$$

where $F_0$, the bulk formation factor, and $\sigma_s$, the surface conductivity, are two free parameters. The formation factor describes the pore space of the particular crushed sample used. The surface conductivity is an intrinsic parameter of the rock, describing the nature of the interface between the minerals constituting the rock, and the electrolyte.

The function $H$ is given by (Revil et al. 1999b) :

$$H(\xi) = 1 - t_+ + F_0\xi + \frac{1}{2}(t_+ - \xi)\left(1 - \frac{\xi}{t_+} + \sqrt{\left(1 - \frac{\xi}{t_+}\right)^2 + \frac{4F_0\xi}{t_+}}\right) \quad (2)$$

**Table 1: Comparison of some water parameters for a few hot springs located at the MCT zone in central Nepal.**

| Hot spring | Temperature (°C) | Conductivity at 25°C (μS/cm) | pH |
|---|---|---|---|
| Tatopani-Kodari | 39.5±0.5 | 847±8 | 6.60±0.02 |
| Syabru Bensi | 61.4±0.5 | 1990±40 | 6.66±0.02 |
| | 46.8±0.5 | 1880±40 | 7.20±0.02 |
| | 34.4±0.5 | 1490±30 | 6.60±0.02 |
| | 32.6±0.5 | 1410±30 | 6.12±0.02 |
| Chilime | 41.4±0.5 | 351±3 | 7.10±0.02 |

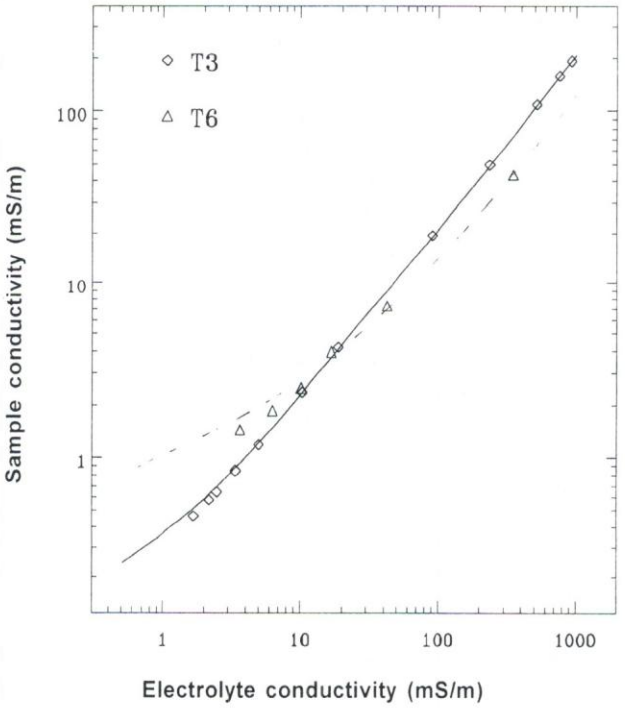


**Fig. 3: Rock sample conductivity as a function of KCl electrolyte conductivity. Results obtained with T1, T2, T4 and T5 are similar to T3 (Table 2). The full line corresponds to the RG equation with $\sigma_s$=0.12 mS/m and the dashed line to the RG equation with $\sigma_s$=1.19 mS/m.**

where $t$ is the "pore fluid Hittorf number" of the cations ($t$ =0.51 for KCl). A combined fit of Eq. (1) to the data yields the values of $F_0$ and $\sigma_s$. As illustrated in Fig. 3, this equation gives a good fit to the data. The obtained values of the surface conductivity are presented in Table 2. They are small for the five samples (T1 to T5) collected north of the MCT, with an average value of 0.13±0.03 mS/m. The value obtained for the sample T6 collected south of the MCT is significantly larger (1.19±0.13 mS/m), and this is already visible from the raw data shown in Fig. 3. This fact may indicate a significant difference in the surface conductivity of Indian crust metasediments compared with gneiss from the Tibetan slab.

**Table 2: Measured characteristics of the rock samples collected at the MCT zone near Tatopani-Kodari (Fig. 2).**

| | T1 | T2 | T3 | T4 | T5 | T6 |
|---|---|---|---|---|---|---|
| **Mineralogy:** **Main components** | quartz muscovite | quartz muscovite anorthite | quartz muscovite | quartz muscovite | quartz muscovite albite | quartz muscovite |
| **Minor components** | albite | amphibole | | albite | | microcline |
| **Accessory minerals** | chlorite | chlorite | | amphibole | | amphibole |
| **Surface conductivity (mS/m)** | 0.11±0.07 | 0.13±0.19 | 0.12±0.05 | 0.13±0.05 | 0.14±0.05 | 1.19±0.13 |
| **Average $\zeta$ potential (mV)** | -26.1±0.6 | -41.2±1.0 | -37.1±1.1 | -16.3±0.2 | -32.3±0.4 | -37.8±1.0 |
| **Parameter $\beta$ in $\zeta \propto \rho_f^{\beta}$** | -0.06±0.10 | 0.15±0.17 | 0.32±0.10 | -0.02±0.04 | 0.09±0.06 | 0.02±0.08 |

On the basis of one sample only, however, it is premature to draw any definite conclusion.

With the same experimental set-up (Lorne et al. 1999a) the electrolyte can be circulated through the crushed sample and the SPC is measured using the relationship :

$$\Delta V = C_s \Delta p \tag{3}$$

where $C_s$ is the SPC, $\Delta V$ is the electric potential difference and $\Delta p$ is the pressure drop across the sample. The voltage reference is taken at the high pressure end (Lorne et al. 1999a). The results as a function of electrolyte resistivity are shown in Fig. 4a for the six rock samples, and compared with the values obtained with Fontainebleau sandstone (Lorne et al. 1999a). For an electrolyte resistivity of 10 Ωm, the values of the SPC are similar for all samples with an average value around 10 mV/0.1MPa, but vary from 200 to 2000 mV/0.1MPa for an electrolyte resistivity of 800 Ωm.

The dependence of the SPC on electrolyte resistivity $\rho_f$ can be written (Revil et al. 1999b; Lorne et al. 1999a; Jouniaux and Pozzi 1995) :

$$C_s = -\frac{\varepsilon}{\eta}\rho_f \zeta \frac{F}{F_0} = -\frac{\varepsilon}{\eta}\rho_f \zeta \frac{1}{H(\xi)} \tag{4}$$

where $\varepsilon$ is the permittivity of the rock and $\eta$ the dynamic viscosity of water. The parameter $\zeta$ describes the interface between the electrolyte and the mineral (Revil et al. 1999a) and $F$ is the formation factor $\sigma_f/\sigma_r$. The $\zeta$ potential can be obtained using Eq. (4) from the measured SPC, i.e. the $C_s$ value, taking into account the correction factor $F/F_0$. The measured $F/F_0$ is shown in Fig. 4b as a function of electrolyte resistivity. It is an important correction for sample T6 because of its higher surface conductivity.

The inferred $\zeta$ potential is shown in Fig. 4c as a function of electrolyte resistivity for the six samples. The average $\zeta$ potential values, given in Table 2, vary from –16.3±0.2 mV for sample T4 to -41.2±0.2 mV for sample T2. The $\zeta$ potential seems independent of $\rho_f$ except for sample T3, for which a significant slope is observed (Fig. 4c). If the variation of the $\zeta$ potential is assumed in the form $\rho_f^b$, then $\beta$ is measured to be 0,32±0.11 for T3, whereas it is compatible with zero for the other samples (Table 2). For Fontainebleau sandstone, $\beta$=0.23±0.01 (Lorne et al. 1999a).

One may object that measurements with crushed samples may not be representative of the conditions of intact rocks, especially the electrical properties which depend on the subtle equilibrium between mineral surfaces and the electrolyte. In the case of Fontainebleau sandstone, a reduction of about 40% was indeed observed for intact samples compared with crushed samples for an electrolyte resistivity of 400 Ωm, but no significant difference was observed for an electrolyte resistivity smaller than 100 Ωm (Lorne et al. 1999b). In this paper, pending a better understanding of such effects, we shall assume that the values measured with crushed samples can be used for intact rocks.

## EVALUATION OF THE ELECTRICAL PARAMETERS OF THE SYSTEM

To estimate the electric potential associated with the water flow at the MCT, some reasonable estimates of the rock parameters are needed as a function of the permeability. In this study, permeability values ranging from 1 D ($10^{-12}$ m$^2$) to 1 mD ($10^{-15}$ m$^2$) will be considered.

The rock resistivity is estimated using the RG equation (Eq. 1). The bulk formation $F_0$ is assumed to depend on the permeability $k$ with a power law of the form $k^q$. The value of the $q$ parameter can be taken from experimental measurements. The value $q$=-0.32 is obtained from volcanic samples (Jouniaux et al. 2000) with $F_0$=200 at k=1 mD. The surface conductivity in Eq. (1) will be assumed to be independent of the permeability, with the values measured in the laboratory (Table 2). This assumption may not be valid, but potential variations of $\sigma_s$ with permeability (Revil et al. 1999b) have not been studied experimentally and are beyond the scope of the present study. With these assumptions, the expected rock resistivity is shown as a

function of permeability in Fig. 5a. The effect of the larger surface conductivity is evident for sample T6 as its resistivity becomes significantly smaller than the other samples for low permeability. The effect of the $q$ parameter can also be seen in Fig. 5a, where the curves obtained with $q$=-0.45 are also shown. Such a value is suggested by experimental data and numerical models (Bernabé 1995). The effect of changing the value of the $q$ parameter is small compared with the effect of the surface conductivity. It is, therefore, important to take into account the surface conductivity of rocks. For values of permeability smaller than 10 mD and surface conductivity larger than 1 mS/m, the rock conductivity is dominated by surface conduction.

To estimate the value of the SPC as a function of permeability, Eq. (5) is used with the previously determined values of the rock resistivity, and the results are shown in Fig. 5b. The electrolyte resistivity has been assumed to be 12 Ωm, the value of the Tatopani-Kodari hot spring (Table 1). The average values of the ζ potential (Table 2) are used, neglecting possible variations with electrolyte resistivity. Possible additional variation of ζ with permeability (Lorne et al. 1999b; Bernabé 1998) are not taken into account. The variations of the SPC with permeability are then only due to the $1/H(\zeta)$ term in Eq. (4), namely the effect of surface conductivity. Even for small values of the surface conductivity (samples T1 to T5), reductions of the SPC by about 50% are observed for a permeability of 1 mD compared with 1 D (Fig. 5b). The effect is even stronger for sample T6 which has a larger surface conductivity. Over the considered range for the permeability, the expected SPC can vary from 4 mV/0.1MPa to 35 mV/0.1MPa.

In this model, the rock resistivity and the value of the SPC are not independent. They are constrained by the experimental measurements and reasonable assumptions, as shown in Fig. 6. Such constraints are important to take into account because not all possible combinations of parameter values are acceptable physically. The variations of the SPC

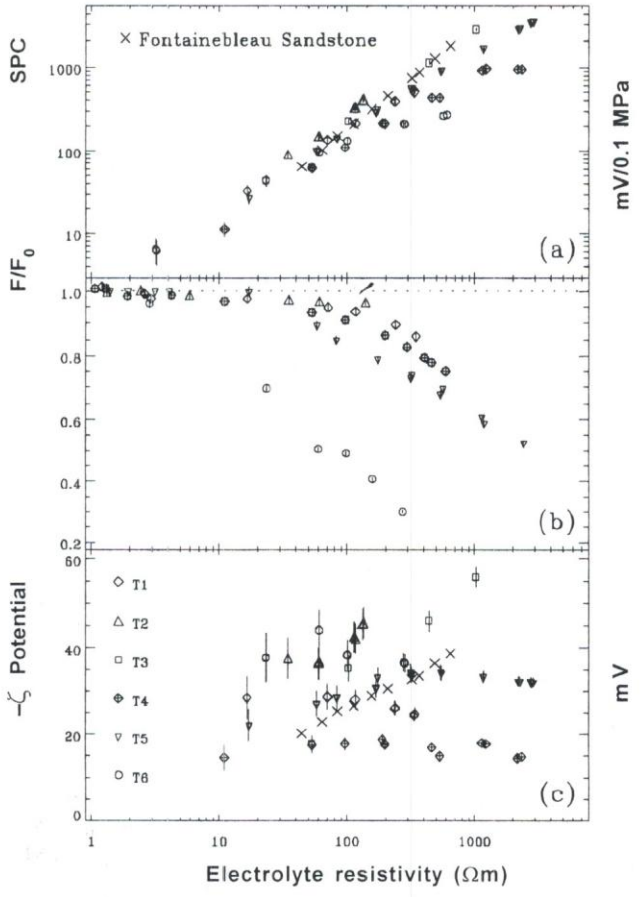


**Fig. 4: Streaming potential coefficient (a), correction factor $F/F_0$ (b), and inferred ζ potential (c) as a function of KCl electrolyte conductivity for the six rock samples collected at the MCT zone (Fig. 2). These data are compared with the values obtained with Fontainebleau sandstone (Lorne et al. 1999a).**

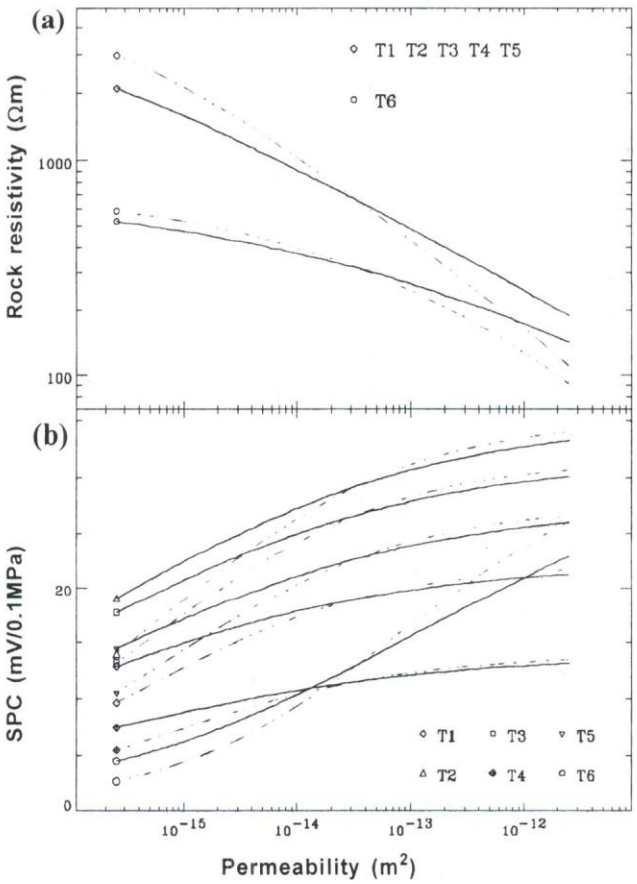


**Fig. 5: Expected rock resistivity (a) and streaming potential coefficient (b) as a function of permeability for the various rock samples. The electrolyte resistivity is 12 Ωm. Equation (1) is used with the surface conductivity values measured in the laboratory (Table 2). The SPC is calculated using Eq.(5) for the values of the ζ potential listed in Table 2. The formation factor is assumed to be of the form $200(k/1\ \text{mD})^q$. The full line corresponds to $q$=-0.32 (Jouniaux et al. 2000). The dashed line correspond to $q$=-0.45 (Bernabé 1995).**

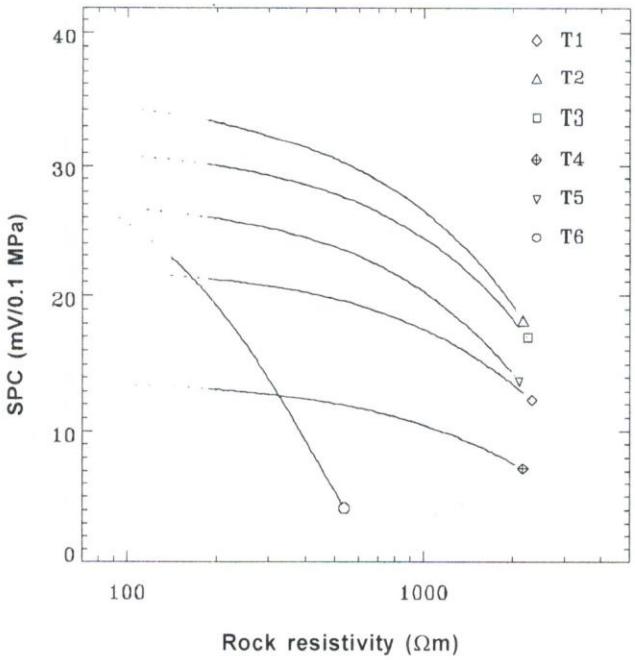


**Fig. 6: Expected streaming potential coefficient as a function of expected rock resistivity for the various rock samples.**

with temperature are not considered here. They should not affect the size of the coupling coefficient by more than 50% (Revil et al. 1999b).

## CALCULATION OF THE ELECTRIC POTENTIAL

The electric potential $V$ and the pore pressure field $p$ are linearly related to the seepage velocity $u$ and the electric current density $J$ (Ishido and Mizutani 1981; Revil et al. 1999b):

$$\begin{pmatrix} u \\ J \end{pmatrix} = M \begin{pmatrix} \nabla p \\ \nabla V \end{pmatrix} \tag{5}$$

where $M$ is the matrix of coupling parameters of the medium (Adler et al. 1999):

$$M = \begin{pmatrix} -\frac{k}{\eta} & -\alpha \\ -\alpha & -\sigma_r \end{pmatrix} \tag{6}$$

The electroosmotic coupling coefficient $\alpha$ is related to the SPC : $\alpha=\sigma_r C_s$. In steady state conditions, the current density $J$ and the seepage velocity have to satisfy differential equations $div(J)=0$ and $div(u)=0$ and are constrained by boundary conditions (Adler et al. 1999). In general, this is a complex coupled problem which can be addressed only numerically (Ishido and Pritchett 1999; Jouniaux et al. 1999). In this paper, a simplified model will be used for which analytical solutions can be found. The purpose of this calculation is to estimate the effect on the SP anomaly of the combined water and electric current distributions in the medium. This calculation does not attempt a full description of the temperature driven buoyancy upwelling at the MCT associated with the gravitational water flow from Tibet (Fig. 1).

Let us consider that the MCT contact zone is two-dimensional and is represented by a vertical slab of fractured material, of thickness $h$ and height $L$, inserted between two different porous media p and p' (Fig. 1) (Adler et al. 1999). The 2D approximation is justified by the cylindrical symmetry of the Himalayan collision compared with the scale of our system (Pandey et al. 1999). Water is percolating in the porous medium north of the fault and is drained to the surface by the higher permeability of the fault. Some fraction of the flow can cross the fault and continue to the south. No flow takes place across the horizontal plane in the porous media north and south of the fault. The layer of height $L$ is assumed to rest on a semi-infinite impermeable space with high resistance. This approximation is justified because the crust exhibits high resistivity and low permeability for depth larger than 5 km. Deep conductors evidenced in MT sounding (Lemonnier et al. 1999) are not likely to affect our conclusions.

For the given boundary conditions for flow and current, the electric potential and pressure field distributions can be solved analytically (see Appendix). Velocity and electric current lines are shown in Fig. 7 with $h$=10 m and $L$=2 km. This analytical model can be considered as a reasonable first approximation for the effect that could be expected at the MCT from the geothermal circulation. The permeability of the fault is assumed to be $k_f$=0.1 D, and the permeability of the porous media $k_p$ and $k_p'$ equal to 1 mD. The chosen values for $L$ and $k_f$ are similar to those proposed for a geothermal system in France (Vasseur et al. 1997).

The current flows at the boundaries $I_f$, $I_p$ and $I_p'$ are assumed to be zero. The integrated water flow rate across the fault is also assumed to be zero, and the value of $Q_f$=$Q_p$ (Fig. 1) is constrained by the experimentally measured flow rate of 3 liter/s in Tatopani-Kodari. We will further assume that only half of the flow rate is available at the spring, and half is lost in diffuse exhausts. In the direction perpendicular to the 2D model, we will assume that the Tatopani spring samples have a width equal to the width of the Bhote-Kosi valley (10 km). The boundary condition is then $Q_f$=-6 x $10^{-7}$ m²/s.

The rock parameters are selected according to the results of the measurements in the laboratory, and the models for extrapolation to the field conditions are shown in Fig. 5 and 6. If T3 is taken as a model for the fault material, a SPC of 28 mV/0.1MPa and a resistivity of 200 Ωm are expected for $k_f$=0.1 D. If T1 is taken as a model of the material north of the fault, a SPC of 14 mV/0.1MPa and a resistivity of 2000 Ωm are expected for 1 mD. For the material south of the fault, the results obtained for T6 indicate a SPC of 6 mV/0.1MPa and a resistivity of 500 Ωm for 1 mD.

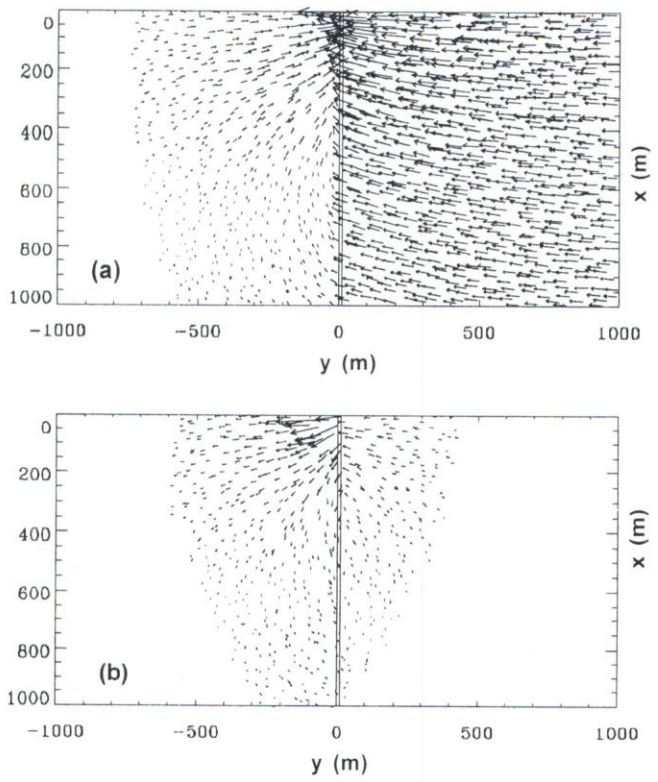


**Fig. 7: Distribution of seepage velocity (a) and electric current (b) for the flow drainage producing hot springs at the MCT. The fractured fault zone is assumed to have a width of $h$=10 m, a height of $L$=2 km, a permeability of 0.1 D, an electrical resistivity of 200 Ωm and a SPC of 28 mV/0.1MPa. The porous media p is assumed to have a permeability of 1 mD, an electrical resistivity of 2000 Ωm and a SPC of 14 mV/0.1MPa. The porous media p' is assumed to have a permeability of 1 mD, an electrical resistivity of 500 Ωm and a SPC of 6 mV/0.1MPa.**

## DISCUSSION

With this choice of parameters, a positive anomaly is observed at the MCT with an amplitude of about 20 mV (Fig. 8), as is expected for upwelling circulation (Zohdy et al. 1973; Revil et al. 1999b). A linear variation of the potential is predicted north of the fault, with a slope of about -50 mV/km. This effect associated with the percolating water north of the MCT is similar to the "topographic effect" in SP (Corwin and Hoover 1979).

The predicted amplitude of the anomaly (20 mV in Fig. 11) is reasonable. A rough estimate of the anomaly associated with geothermal circulation is (Revil and Pezard 1998):

$$V(0) = \alpha_w \rho_w g \Delta T C_f L \tag{7}$$

where $\Delta T$ is the thermal gradient, $g$ the acceleration of gravity, $\alpha_w$ the thermal volume expansion coefficient of water, and $\rho_w$ the water density. Taking $\Delta T$=40°C for the high permeability fault zone, $\alpha_w$=$10^{-3}$ $K^{-1}$, $\rho_w$=$10^3$ Kg/m$^3$, $C_f$=28 mV/0.1MPa=2.8 $10^{-7}$ V/Pa, gives $V(0)$= 224 mV. The size of the anomaly in our calculation is reduced compared with this expectation because of leakage currents in the imbedding medium and a progressive feeding of the fault by the side instead of an upwelling column assumed for Eq. (7).

An estimate of the flow rate can also be obtained assuming no pressure in excess of hydrostatic pressure (Revil and Pezard 1998):

$$Q_T = \frac{k_f h}{\eta} \alpha_w \rho_w g \Delta T \tag{8}$$

This estimate gives 4x$10^{-7}$ m$^2$/s, and is certainly compatible, given the largely unknown value of the product $h.k_f$, with the value 6x$10^{-7}$ m$^2$/s obtained above from the measured flow rate. Equation (8) could have been grossly wrong if there is a large excess pressure, for example, associated in our case (Fig. 1) with the topographic gradient. It does not seem to be the case. This comparison rather suggests that the estimated value of the anomaly in Eq. (7) is an overestimate.

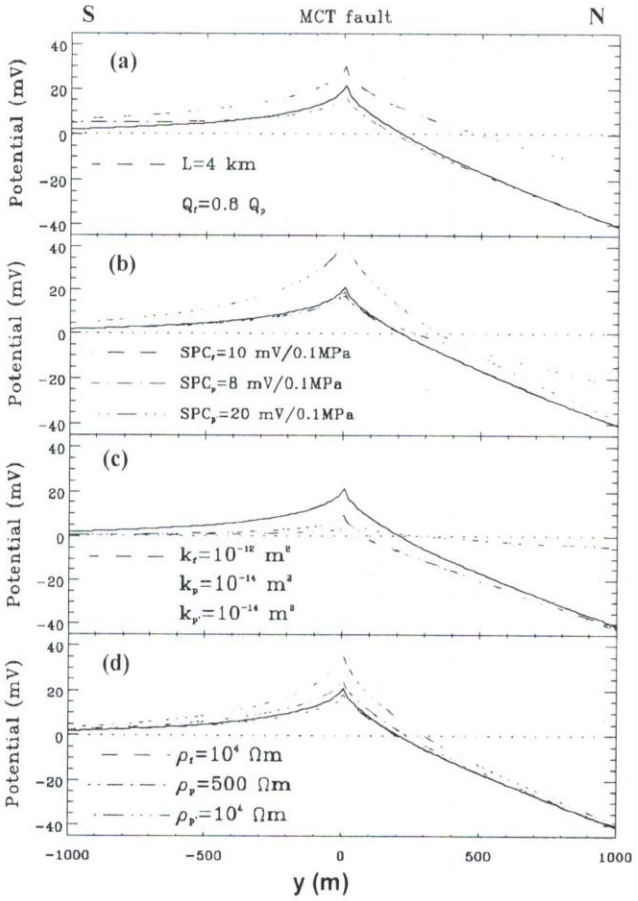


**Fig. 8: The calculated electric potential on surface as a function of distance across the MCT: a) Effect of changing boundary conditions ; b) Effect of changing values of the SPC ; c) Effect of changing the value of permeability ; d) Effect of changing the value of rock resistivity. Default values of parameters are given in Fig. 7.**

The effect of the various parameters can be studied in detail with the analytical model. In Fig. 8a, the effect of doubling the height $L$ is shown. The size of the anomaly is roughly increased by 50% because, for fixed permeability, an increased pressure is required to sustain the same vertical seepage flow rate in the fault. If 20% of the water crosses the fault to the south, the amplitude of the anomaly is reduced by a factor of 2 with respect to some reference point at 1 km south of the fault, but is almost unchanged with respect to any point located north of the fault. In Fig. 8c the effect of changing the permeability values is shown. The size of the anomaly is directly proportional to the assumed value of the permeability of the fault. The permeability values in the imbedding media have a smaller but has significant effect on the size of the anomaly. This illustrates the fact that flow leakage does affect the electrical potential in the coupled problem.

The effect of changing the values of the SPC is shown in Fig. 8b. If the value of the SPC of the fault is 10 mV/0.1MPa, which is the smallest measured value at a permeability of 1 D (sample T4 in Fig. 5b), then the anomaly is reduced by 15%. The effect of changing the SPC in the porous medium has an effect on the slope north of the fault, but virtually no effect on the amplitude of the anomaly. Increasing the SPC south of the fault from 6 mV/0.1MPa to 20 mV/0.1MPa, the highest value suggested by the laboratory measurement (sample T2), increases the anomaly significantly. This calculation demonstrates that, to obtain a result beyond an order of magnitude estimate, it is necessary to properly model the distribution of leakage currents with proper values for the coupling coefficients of the imbedding media. The effect of changing the relative values of rock resistivity is also significant (Fig. 8d). Current leakage in the embedding medium south of the fault reduces the amplitude of the anomaly by about a factor of 2.

Bounds for the expected value of the anomaly versus the permeability of the fault are shown in Fig. 9. The anomaly could be as high as 100 mV, for a fault permeability of $10^{-13}$ $m^2$. Tthe need of taking into account the surface conductivity of the rock may be noted in Fig. 9. The anomaly predicted with sample T6 could be high at high permeability and lower than other rocks at low permeability. Furthermore, a slight change in the dependence of the formation factor with permeability can change the predicted anomaly by more than 50%.

This study is a first step in the estimation of electric effect associated with hydrothermal circulation in a tectonically active setting. The main uncertainty in estimating the amplitude of the anomaly are the permeability and the size of the fault. Although the product $k/h$ is constrained by the flow rate, a large uncertainty still remains. A way to estimate the value of the permeability independent of the observed flow rate is desired. Although the value of 0.1 D used in this work for a fault width of 10 m seems reasonable, further experimental evidence is required. The use of the analytical model allowed us to quantify other uncertainties in the calculation of the anomaly, and in particular, the influence of water leakage across the fault, or the combined effects of flow and current leakage in the imbedding media. Reasonable values have to be used for the SPC. For the present study, we tried to constrain the values of the SPC with experimental measurements in the laboratory but we still rely on a poorly known extrapolation as a function of permeability. Dedicated studies are needed to establish the validity of such extrapolations to fit with the experimental data.

Keeping these uncertainties in mind, the amplitude of the anomaly predicted by our analytical model varies from 1 mV to at most 100 mV, with a most likely value estimated of the order of 20 mV. It should be remembered during field experiment that the expected that these expected amplitudes remain small. Experimentally, SP profiling around the Tatopani-Kodari was attempted by the authors but no conclusive results could be obtained because of large surface noise. This noise was partly due to highly resistive layers near the surface, and to perturbations due to local surface seepage, flash rains or due to the vegetation. Measuring local anomalies of the order of 20 mV appears as a challenge in this context. It is therefore unlikely that SP variations at Tatopani-Kodari, or similar sites near the MCT such as Syabru Bensi or Chilime, could give relevant clues on the time evolution of pore pressure at depth in association with stress accumulation, unless other mechanisms beyond streaming potentials take place.

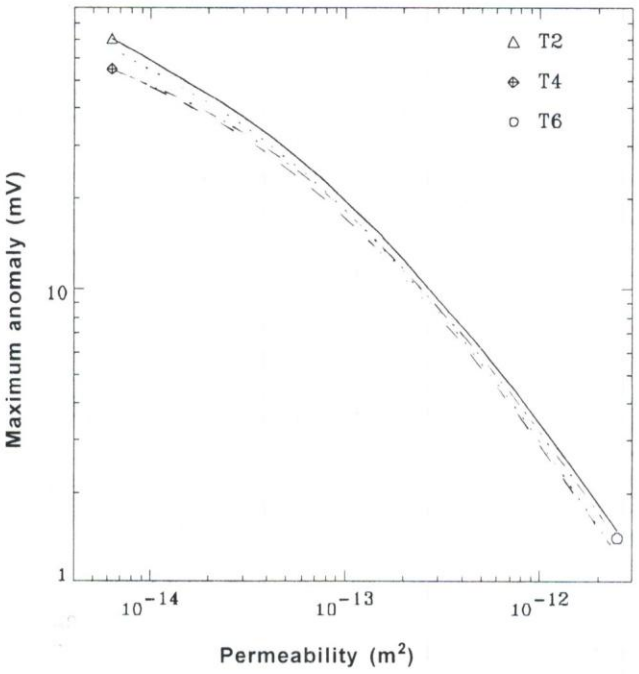


**Fig. 9: The maximum anomaly as a function of the permeability of the fault. The resistivity of the fault and its SPC vary as a function of the permeability according to the models of Fig. 7 and 8, taking T2, T4 and T6 as typical examples with $q$=-0.32. The dotted line corresponds to T6 with $q$=-0.45.**

## ACKNOWLEDGEMENTS

The authors are grateful to N. R. Sthapit, R. P. Tandukar and M. R. Pandey of the Department of Mines and Geology for support and encouragement. Stefan Brüggerhoff and Dirk Kirchner from the German Mining Museum in Bochum, Germany, are thanked for their kind X-ray analysis of the rock samples. This paper greatly benefited from the inspiring comments and detailed suggestions of one anonymous reviewer.

## REFERENCES

Adler, P. M., Le Mouël, J.-L. and Zlotnicki, J., 1999, Electrokinetic and magnetic fields generated by flow through a fractured zone : a sensitivity study for La Fournaise volcano. Geophys. Res. Lett., v. 26, pp. 795-798.

Bernabé, Y., 1995, The transport properties of networks of cracks and pores. Jour. Geophys. Res., v. 100, pp. 436-4231-2141.

Bernabé, Y., 1998, Streaming potential in heterogeneous networks. Jour. Geophys. Res., v. 103 B9, pp. 20,827–20,841.

Bhattarai, D. R., 1980, Some geothermal springs of Nepal. Tectonophysics, v. 62, pp. 7–11.

Bilham, R., Blume, F., Bendick, R. and Gaur, V. K., 1998, Geodetic constraints on the translation and deformation of India : implications for future great Himalayan earthquakes. Current Science, v. 74, pp. 213–229.

Bogoslovsky, V. A. and Ogilvy, A. A., 1970, Natural potential anomalies as a quantitative index of the rate of seepage from water reservoirs. Geophysical Prospecting, v. 18, pp. 261–268.

Cattin, R., Martelet, G., Henry, P., Avouac, J.-P., Diament, M., and Shakya, T. R., 2001, Gravity anomalies, crustal structure and thermo-mechanical support of the Himalaya of Central Nepal. Geophys. Jour. Int., v. 147, pp. 381–392.

Corwin, R. F. and Hoover, D. B., 1979, The self-potential method in geothermal exploration. Geophysics, v. 44, pp. 226–245.

Corwin, R. F. and Morrison, H. F., 1977, Self-potential variations preceding earthquakes in central California. Geophys. Res. Lett., v. 4, pp. 171–174.

Geller, R., Editor, 1996, Debate on «VAN», Special issue. Geophys. Res. Let., v. 23, pp. 1291–1452.

Guillot, S., 1999, An overview of the metamorphic evolution in Central Nepal. Jour. Asian Earth Sciences, v. 17, pp. 713–725.

Ishido, T. and Mizutani, H., 1981, Experimental and theoretical basis of electrokinetic phenomena in rock-water systems and its applications to geophysics. Jour. Geophys. Res., v. 86, pp. 1763–1775.

Ishido, T. and Pritchett, J. W., 1999, Numerical simulation of electrokinetic potentials associated with subsurface flow. Jour. Geophys. Res., v. 104 B7, pp. 15,247–15,529.

Jouniaux, L. and Pozzi, J.-P., 1995, Streaming potential and permeability of saturated sandstones under triaxial stress : Consequences for electrotelluric anomalies prior to earthquakes. Jour. Geophys. Res., v. 100, pp. 10,197–10,209.

Jouniaux, L., Bernard, M. L., Pozzi, J.-P. and Zamora, M., 2000, Streaming potential in volcanic rocks from Mount Pelée. Jour. Geophys. Res., v. 105, pp. 8391–8401.

Jouniaux, L., Pozzi, J.-P., Berthier, J. and Massé, P., 1999, Detection of fluid flow variations at the Nankai trough by electric and magnetic measurements in boreholes or at the sea floor. Jour. Geophys. Res., v. 104 B12, pp. 29,293–29,309.

Lemonnier, C., Marquis, G., Perrier, F., Avouac, J.-P., Chitrakar, G., Kafle, B., Sapkota, S., Gautam, U., Tiwari, D. and Bano, M., 1999, Electrical structure of the Himalay of Central Nepal : high conductivity around the mid-crustal ramp along the MHT. Geophys. Res. Lett., v. 26, pp. 3261–3264.

Lorne, B., Perrier, F. and Avouac, J.-P., 1999a, Streaming potential measurements, I : Properties of the electrical double layer from crushed rock samples. J. Geophys. Res., v. 104 B8, pp. 17,857–17,877.

Lorne, B., Perrier, F. and Avouac, J.-P., 1999b, Streaming potential measurements, II : Relationship between electrical and hydraulic flow patterns from rock samples during deformation. Jour. Geophys. Res., v. 104 B8, pp. 17,879–17,896.

Madhikarmi, D. P., 1980, Geological map around Bhote Kosi and Balephi Khola. Map published by Department of Mines and Geology, Kathmandu, Nepal.

Marino, S., Coelho, D., Bekri, S. and Adler, P. M., 2000, Electroosmotic phenomena in fractures. J. Colloid Interface Sci., v. 223, pp. 292–304.

Massenet, F. and Pham, V. N., 1985, Experimental and theoretical basis of self-potential phenomena in volcanic areas with reference to results obtained on Mount Etna (Sicily). Earth. Planet. Sci. Lett., v. 73, pp. 415–429.

Michel, S. and Zlotnicki, J., 1998, Self-potential and magnetic surveying of La Fournaise volcano (Réunion Island): correlations with faulting, fluid circulation, and eruption. Jour. Geophys. Res., v. 103 B8, pp. 17,845–17,857.

Mizutani, H., Ishido, T., Yokokura, T. and Ohnishi, S., 1976, Electrokinetic phenomena associated with earthquakes, Geophys. Res. Lett., v. 3, pp. 365–368.

Morat, P. and Le Mouël, J.-L., 1992, Electrical signals generated by stress variations in porous non saturated rocks. C. R. Acad. Sci. Paris, v. 315, pp. 955–963.

Morat, P., Le Mouël, J.-L. and Zlotnicki, J., 1989, Electrical signals generated by the collapse of the pillars of a gypsum quarry. C. R. Acad. Sci. Paris, v. 308, pp. 33–38.

Ogilvy, A. A., Ayed, M. A. and Bogoslovsky, V. A., 1969, Geophysical studies of water leakages from reservoirs. Geophysical Prospecting, v. 17, pp. 36–62.

Pandey, M. R., Tandukar, R. P., Avouac, J.-P., Lavé, J. and Massot, J.-P., 1995, Interseismic strain accumulation on the Himalayan crustal ramp (Nepal). Geophys. Res. Lett., v. 22, pp. 751–754.

Pandey, M. R., Tandukar, R. P., Avouac, J.-P., Vergne, J. and Héritier, T., 1999, Seismotectonics of the Nepal Himalaya from a local seismic network. Jour. Asian Earth Sciences, v. 17, pp. 703–712.

Pengra, D. B., Li, S. X. and Wong, P. Z., 1999, Determination of rock properties by low-frequency AC electrokinetics. Jour. Geophys. Res., v. 104, pp. 29485–29508.

Perrier, F., Petiau, G., Clerc, G., Bogorodsky, V., Erkul, E., Jouniaux, L., Lesmes, D., Macnae, J., Meunier, J., Morgan, D., Nascimento, D., Oettinger, G., Schwarz, G., Toh, H., Valiant, M., Vozoff, K. and Yazici-Çakin, O., 1997, A one-year systematic study of electrodes for long period measurement of the electric field in geophysical environments. Jour. Geomag. Geoelec., v. 49, pp. 1677–1696.

Perrier, F. and Morat, P., 2000, Characterization of electrical daily variations induced by capillary flow in the non-saturated zone. Pure appl. Geophys., v. 157, pp. 785–810.

Perrier, F., Trique, M., Aupiais, J., Gautam, U. and Shrestha, P., 1999, Electric potential variations associated with periodic spring discharge in Western Nepal. C. R. Acad. Sci. Paris, v. 328, pp. 73–79.

Perrier, F., Trique, M., Lorne, B., Avouac, J.-P., Hautot, S. and Tarits, P., 1998, Electric potential variations associated with lake level variations. Geophys. Res. Lett., v. 25, pp. 1955–1958.

Pham, V. N., Boyer, D., Chouliaras, G., Le Mouël, J.-L., Rossignol, J.-C. and Stavrakakis G. N., 1998, Characteristics of electromagnetic noise in the Ioannina region (Greece) ; a possible origin for so called "Seismic Electric Signal" (SES). Geophys. Res. Lett., v. 25, pp. 2229–2232.

Pham, V. N., Boyer, D., Perrier, F. and Le Mouël, J.-L., 2001, Generation mechanisms of telluric noises in ULF band : possible sources for the so-called « Seismic Electric Signals » (SES). C. R. Acad. Sci. Paris, v. 333, pp. 255–262.

Pisarenko, D., Morat, P. and Le Mouël, J.-L., 1996, On a possible mechanism of sandstone alteration: evidence from electric potential measurements. C. R. Acad. Sci. Paris, v. 322, pp. 17–24.

Raleigh, B., Molnar, P., Hanks, T., Nur, A., Savage, J., Craig, H., Turner, R. and Bennett, G., 1977, The prediction of the Haicheng earthquake. EOS Trans. Am. Geophys. Union, v. 58, pp. 236–272.

Revil, A. and Glover, P. W. J., 1998, Nature of surface electrical conductivity in natural sands sandstones, and clays. Geophys. Res. Lett., v. 25, pp. 691–694.

Revil, A., and Pezard, P. A., 1998, Streaming electrical potential anomaly along faults in geothermal areas. Geophys. Res. Lett., v. 25, pp. 3197–3200.

Revil, A., Pezard, P. A. and Glover, P. W. J., 1999a, Streaming potential in porous media 1. Theory of the zeta potential. Jour. Geophys. Res., v. 104, pp. 20,021–20,031.

Revil, A., Schwaeger, H., Cathles III, L. M. and Manhardt, P. D., 1999b, Streaming potential in porous media 2. Theory and application to geothermal systems. Jour. Geophys. Res., v. 104, pp. 20,033–20,048.

Thony, J.-L., Morat, P., Vachaud, G. and Le Mouël, J.-L., 1997, Field characterization of the relationship between electrical potential gradients and soil water flux. C. R. Acad. Sci. Paris, v. 325, pp. 317–321.

Trique, M., Richon, P., Perrier, F., Avouac, J.-P. and Sabroux, J.-C., 1999, Radon emanation and electric potential variations associated with transient deformation near reservoir lakes. Nature, v. 399, pp. 137–141.

Upreti, B. N., 1999, An overview of the stratigraphy and tectonics of the Nepal Himalaya. Jour. Asian Earth Science, v. 17, pp. 577–606.

Varotsos, P., Alexopoulos, K. and Lazaridou, M., 1993, Latest aspects of earthquake prediction in Greece by seismic electric signals, II. Tectonophysics, v. 224, pp. 1–37.

Vasseur, G., Michard, G. and Fouillac, C., 1997, Further study of the deep structure and hydrodynamics of an active hydrothermal system (Chaudes-Aigues, France). Hydrogeology, v. 4, pp. 3–17.

Yoshida, S., 2001, Convection current generated prior to rupture in saturated rocks. J. Geophys. Res., v. 106 B2, pp. 2103–2120.

Zlotnicki, J. and Le Mouël, J.-L., 1990, Possible electrokinetic origin of large magnetic variations at La Fournaise Volcano. Nature, v. 343, pp. 633–636.

Zohdy, A. A. R., Anderson, L. A. and Muffler, L. J. P., 1973, Resistivity, self-potential, and induced-polarization surveys of a vapor-dominated geothermal system. Geophysics, v. 38, pp. 1130–1144.

## APPENDIX

The solutions of the model depicted in Fig. 1 can be written by analogy with (Adler et al. 1999) :

$$p_p = \Delta y + \sum_{n=0}^{\infty} \bar{a}_n \cos\frac{n\pi x}{L}\exp\left(-\frac{n\pi y}{L}\right) \quad \text{(A1)}$$

$$V_p = \Gamma y + \sum_{n=0}^{\infty} \bar{c}_n \cos\frac{n\pi x}{L}\exp\left(-\frac{n\pi y}{L}\right) \quad \text{(A2)}$$

$$p_f = B\sin\frac{\pi x}{2L}\exp\left(\frac{\pi y}{2L}\right) + \sum_{n=0}^{\infty} b_n \cos\frac{n\pi x}{L}\exp\left(\frac{n\pi y}{L}\right) + \sum_{n=1}^{\infty} \bar{b}_n \cos\frac{n\pi x}{L}\exp\left(-\frac{n\pi y}{L}\right) \quad \text{(A3)}$$

$$V_f = D\sin\frac{\pi x}{2L}\exp\left(\frac{\pi y}{2L}\right) + \sum_{n=0}^{\infty} d_n \cos\frac{n\pi x}{L}\exp\left(\frac{n\pi y}{L}\right) + \sum_{n=1}^{\infty} \bar{d}_n \cos\frac{n\pi x}{L}\exp\left(-\frac{n\pi y}{L}\right) \quad \text{(A4)}$$

$$p_p' = \Delta' y + \sum_{n=0}^{\infty} a'_n \cos\frac{n\pi x}{L}\exp\left(\frac{n\pi y}{L}\right) \quad \text{(A5)}$$

$$V_p' = \Gamma' y + \sum_{n=0}^{\infty} c'_n \cos\frac{n\pi x}{L}\exp\left(\frac{n\pi y}{L}\right) \quad \text{(A6)}$$

These functions automatically satisfy the boundary conditions and the relations $\Delta V=0$ and $\Delta p=0$ everywhere in the media. The term $sin(\pi x/2L)exp(\pi y/2L)$ in $p_f$ and $V_f$ is introduced to allow for upwelling flow at x=0. The form of this term is chosen in arbitrary fashion to allow for analytical solutions of the problem with a reasonable physics content. Its exact form is irrelevant when $h$ is small compared with $L$. The constants $\Delta$, $\Gamma$, $B$, $D$, $\Delta'$, $\Gamma'$ are obtained from the boundary conditions :

$$\begin{pmatrix} Q_f \\ I_f \end{pmatrix} = M_f \int_0^h \begin{pmatrix} \nabla p_f \\ \nabla V_f \end{pmatrix}_{x=0} dy \quad \text{(A7)}$$

$$\begin{pmatrix} Q_p \\ I_p \end{pmatrix} = M_p \int_0^L \begin{pmatrix} \nabla p_p \\ \nabla V_p \end{pmatrix}_{y=\infty} dx \quad \text{(A8)}$$

$$\begin{pmatrix} Q'_p \\ I'_p \end{pmatrix} = M'_p \int_0^L \begin{pmatrix} \nabla p'_p \\ \nabla V'_p \end{pmatrix}_{y=-\infty} dx \quad \text{(A9)}$$

with the conditions :

$$Q_p = Q_f + Q'_p \quad \text{(A10)}$$

and:

$$I_p = I_f + I'_p \quad \text{(A11)}$$

The coefficients $\bar{a}_n$, $\bar{c}_n$, $b_n$, $\bar{b}_n$, $d_n$, $\bar{d}_n$, $a'_n$ and $c'_n$ of the expansion are obtained by writing the continuity of $p$ and $V$ and of the normal components of $u$ and $J$ at $y=0$ and $y=h$. The results are given by :

$$a'_n = b_n + \bar{b}_n + Bg_n \tag{A12}$$

$$c'_n = d_n + \bar{d}_n + Dg_n \tag{A13}$$

$$\bar{a}_n E_n^{-1} = b_n E_n + \bar{b}_n E_n^{-1} + Bg_n \chi \tag{A14}$$

$$\bar{c}_n E_n^{-1} = d_n E_n + \bar{d}_n E_n^{-1} + Dg_n \chi \tag{A15}$$

$$\mathrm{M}\begin{pmatrix} b_n \\ \bar{b}_n \\ d_n \\ \bar{d}_n \end{pmatrix} = g_n \begin{pmatrix} B\left(\frac{k'_p}{\eta} - \frac{1}{2n}\frac{k_f}{\eta}\right) + D\left(\alpha'_p - \frac{1}{2n}\alpha_f\right) \\ B\left(\alpha'_p - \frac{1}{2n}\alpha_f\right) + D\left(\sigma'_p - \frac{1}{2n}\sigma_f\right) \\ -\chi B\left(\frac{k_p}{\eta} + \frac{1}{2n}\frac{k_f}{\eta}\right) - \chi D\left(\alpha_p + \frac{1}{2n}\alpha_f\right) \\ -\chi B\left(\alpha_p + \frac{1}{2n}\alpha_f\right) - \chi D\left(\sigma_p + \frac{1}{2n}\sigma_f\right) \end{pmatrix} \tag{A16}$$

where:

$$g_n = \frac{4}{\pi}\frac{1}{1-4n^2} \tag{A17}$$

$$E_n = \exp\left(\frac{n\pi h}{L}\right) \tag{A18}$$

$$\chi = \exp\left(\frac{\pi h}{2L}\right) \tag{A19}$$

$$\mathrm{M} = \begin{bmatrix} \frac{k_f}{\eta} - \frac{k'_p}{\eta} & -\frac{k_f}{\eta} - \frac{k'_p}{\eta} & \alpha_f - \alpha'_p & -\alpha_f - \alpha'_p \\ \alpha_f - \alpha'_p & -\alpha_f - \alpha'_p & \sigma_f - \sigma'_p & -\sigma_f - \sigma'_p \\ \left(\frac{k_f}{\eta} + \frac{k_p}{\eta}\right)E_n & \left(-\frac{k_f}{\eta} + \frac{k_p}{\eta}\right)E_n^{-1} & (\alpha_f + \alpha_p)E_n & (-\alpha_f + \alpha_p)E_n^{-1} \\ (\alpha_f + \alpha_p)E_n & (-\alpha_f + \alpha_p)E_n^{-1} & (\sigma_f + \sigma_p)E_n & (-\sigma_f + \sigma_p)E_n^{-1} \end{bmatrix} \tag{A20}$$

A maximum of 40 terms in the sums of Eq. (A1) to (A6) are used in the calculation, which is sufficient for obtaining a precision better than 1%.